*Inorganica Chimica Acta, 189* (1991) 149–155



# Oxygen catalysis by anhydrous ruthenium(IV) oxide

Andrew Mills* and Hefin L. Davies
*Department of Chemistry, Singleton Park, Swansea SA2 8PP (UK)*

(Received May 15, 1991)

**Abstract**

The results of a kinetic study of the oxidation of water to oxygen by $Ce^{IV}$ ions in different acid media, mediated by anhydrous ruthenium(IV) oxide are described. In an acid medium which is predominantly $HClO_4$ the kinetics are diffusion controlled and first order with respect to both $[Ce^{IV}]$ and $[RuO_2]$ and exhibit an activation energy of 19 kJ $mol^{-1}$. In 0.5 mol $dm^{-3}$ $H_2SO_4$ the kinetics are much slower and complex, the rate decreasing with increasing $[Ce^{III}]$. The kinetics of catalysis observed in all the different acid media studied are readily interpreted using an electrochemical model in which the catalyst particles are considered as acting as microelectrodes which mediate electron transfer between a Nernstian reduction reaction ($Ce^{IV} \rightarrow Ce^{III}$) and an irreversible oxidation reaction ($H_2O \rightarrow 2H^+ + \frac{1}{2}O_2$). This electrochemical model is used to analyse the complex kinetics observed in 0.5 mol $dm^{-3}$ $H_2SO_4$ and extract mechanistic information concerning the nature of the rate determining step.

## Introduction

Oxygen catalysis, along with hydrogen catalysis, is an essential element of any water-splitting, photochemical system [1, 2]. By definition, an oxygen catalyst is able to mediate the oxidation of water to oxygen by an oxidant with a sufficiently positive redox potential (i.e. $E° > (1.23 - 0.059 \times pH)$ V versus NHE. Unfortunately, many materials are either inactive as $O_2$ catalysts, or rendered so by the formation of a passivating oxide layer, upon exposure to the oxidant [3]. In addition, many other materials are themselves readily corroded under the highly oxidising conditions involved. As a result, the number of materials which have been reported as examples of $O_2$ catalysts are limited. The material most often used as an $O_2$ catalyst is ruthenium(IV) oxide, however care must be taken since there are many different forms of this oxide [3]. For example, highly hydrated ruthenium dioxide hydrate ($\%H_2O \geqslant 24\%$), i.e. $RuO_2 \cdot xH_2O$, which is the form most commonly available commercially, is not a good oxygen catalyst, but rather undergoes anodic corrosion to form $RuO_4$ upon exposure to a strong oxidant such as $Ce^{IV}$ ions [4]. In contrast, by annealing $RuO_2 \cdot xH_2O$ in air (or $N_2$, or $O_2$ for that matter, as the nature of atmosphere makes no difference), for 5 h at 144 °C, a partially dehydrated form of $RuO_2 \cdot xH_2O$ is created, which we call *thermally activated ruthenium dioxide hydrate*, or $RuO_2 \cdot yH_2O$* for short, which is both an $O_2$ catalyst and stable towards anodic corrosion [5].

The $O_2$ catalytic activity of partially dehydrated activated ruthenium dioxide hydrate decreases with increasing annealing temperature above 144 °C and associated with this observed loss in activity is a decreasing $\%H_2O$ content, decreasing specific surface area (i.e. surface area per gram) and increasing degree of crystallinity [3, 5]. Finally, samples of $RuO_2 \cdot xH_2O$ annealed at 900 °C appear highly crystalline (rutile structure) dark blue–black powders with no $\%H_2O$ content and of low specific surface area and in all aspects identical to commercial anhydrous ruthenium dioxide, i.e. $RuO_2$. In the course of initial studies on ruthenium(IV) oxides as $O_2$ catalysts, our group [6] reported anhydrous ruthenium(IV) oxide as an example of a corrosion-resistant, but $O_2$ catalytically inactive material, however, this latter description has since proved inappropriate [7]. Anhydrous ruthenium dioxide hydrate is an $O_2$ catalyst, but, because of its very low specific surface area, compared with $RuO_2 \cdot yH_2O$*, a much higher catalyst concentration and reaction temperature must be employed to observe its catalytic action. In this paper we report the results of a kinetic study of oxygen catalysis by anhydrous ruthenium dioxide hydrate.

*Author to whom correspondence should be addressed.

0020-1693/91/$3.50

## Experimental

*Materials*

The anhydrous ruthenium dioxide hydrate used throughout this work was obtained from Johnson Matthey (Batch No. 061199) and, unless stated otherwise, the concentration of the stock dispersion was 300 mg $dm^{-3}$. The procedure for the preparation of a stock dispersion is reported elsewhere [8]. All $Ce^{IV}$ solutions were made up from an Analytical Volumetric Solution of 0.1 mol $dm^{-3}$ $Ce^{IV}$ sulfate solution in 0.5 mol $dm^{-3}$ $H_2SO_4$. The 0.5 mol $dm^{-3}$ $H_2SO_4$ and 1 mol $dm^{-3}$ $HClO_4$ were prepared from their respective concentrated acids. All other chemicals were purchased from BDH in the purest form available (usually AnalaR). The water used to prepare solutions was always doubly distilled and deionised.

*Kinetic studies*

The oxidation of water by $Ce^{IV}$ ions mediated by anhydrous ruthenium dioxide hydrate, i.e.

$$4Ce^{IV} + 2H_2O \xrightarrow{RuO_2} 4Ce^{III} + 4H^+ + O_2 \quad (1)$$

was monitored spectrophotometrically as a function of time using a Perkin–Elmer Lambda 3 spectrophotometer. The absorbance versus time plots were recorded, stored and subsequently analysed using a microcomputer (BBC Masterclass). In a typical experiment 2.5 $cm^3$ of the stock dispersion (made up in either 1 mol $dm^{-3}$ $HClO_4$ or 0.5 mol $dm^{-3}$ $H_2SO_4$) were placed in a 1 cm quartz fluorescence cell which was then positioned in the thermostatted sample cell holder of the double-beam spectrophotometer. The cell contents were stirred continuously at a constant 1000 rpm with a magnetically-driven Teflon-coated flea and the absorbance due to the catalyst dispersion alone allowed to settle down to a constant value, typically 15–20 min. After this period the kinetic run was initiated, via the injection of the $Ce^{IV}$ solution (typically 90 $mm^3$ of 0.1 mol $dm^{-3}$ $Ce^{IV}$ solution in 0.5 mol $dm^{-3}$ $H_2SO_4$) using a gas-tight syringe. Blank runs carried out in the absence of catalyst showed that in all cases mixing was complete within 5 s of the injection being made; this is a negligible time period compared with that of a typical run, i.e. > 50 s.

Redox potential measurements of different $Ce^{IV}/Ce^{III}$ ratios in various acid media were carried out using a Pt/(Ag/AgCl) combination redox electrode (Schott Gerate Pt62).

## Electrochemical model

In many cases of redox catalysis, of which reaction (1) is just one example, it has been established that the role of the catalyst as is an electrode which simply provides a medium through which electrons can be transferred from one redox couple to another [2, 9]. Provided the redox couple is chemically inert under the reaction conditions used and that the redox couples act independently of each other (the Wagner–Traud additivity principle) it is possible to predict the kinetics of catalysis from a knowledge of the current–voltage curves of the two redox couples involved on the redox catalyst and this forms the basis of the electrochemical model of redox catalysis [2, 9].

For most anode materials, including anhydrous $RuO_2$, the electrochemical oxidation of water to $O_2$ is a highly irreversible reaction and, as a result, the associated current–voltage curve is usually described very well by a simple Tafel-type equation [10, 11], i.e.

$$i_{O_2} = i_w \exp(2.303\eta/b) \quad (2)$$

where $i_{O_2}$ is the anodic current flowing through the redox catalyst due to the oxidation of water to $O_2$, $i_w$ is the exchange current for the $O_2/H_2O$ couple, $\eta$ is the overpotential and $b$ is the Tafel slope. The overpotential, $\eta$, is the difference between the applied potential, $E_{ap}$, and the equilibrium potential for the $O_2/H_2O$ couple.

For most materials it is likely that the exchange current density for the $Ce^{IV}/Ce^{III}$ couple is much greater than that of the $O_2/H_2O$ couple. If the exchange current density for the $Ce^{IV}/Ce^{III}$ couple is very large it is likely that the heterogeneous rate constant for electron transfer between $Ce^{IV}$ and $Ce^{III}$ ions, of which the exchange current density is a measure, will be much greater than the mass-transfer coefficient for the $Ce^{IV}$ and $Ce^{III}$ ions ($k_d$). In such a case the current–voltage curve for the $Ce^{IV}/Ce^{III}$ couple will be that for a Nernstian reaction [12] and, therefore, can be expressed as follows:

$$E_{ap} = E'_{Ce} + (RT/F)\ln(i_{Ce} - i_{l,c})/(i_{l,a} - i_{Ce}) \quad (3)$$

where $E'_{Ce}$ is the formal redox potential of the $Ce^{IV}/Ce^{III}$ couple (taken to be 1.444 V versus NHE), $i_{Ce}$ is the current flowing through the redox catalyst due to the reduction of $Ce^{IV}$ ions, and $i_{l,c}$ and $i_{l,a}$ are the limiting cathodic (negative) and anodic (positive) currents, respectively. The constant, $k_d$, depends inversely upon the hydrodynamic flow conditions around the electrode which, in our work, are kept constant by using a fixed rate of stirring.

According to the electrochemical model of catalysis [2, 9] when both redox couples are present the redox catalyst particles adopt a mixture potential, $E_{mix}$, at which the net current flowing through the redox catalyst is zero, i.e.

$$i_{mix} = i_{O_2} = -i_{Ce} \quad (4)$$

where $i_{mix}$ is the mixture current.

In order to test fully the applicability of the electrochemical model described above to a redox catalyst system it is necessary to relate the model parameters, $i_{mix}$ and $E_{mix}$ to the kinetic data. In our work the kinetic data is in the form of a series of absorbance–time profiles. For any kinetic run the rate of reduction of the $Ce^{IV}$ ions at any time $t$, $r(t)$ (units: mol $dm^{-3}$ $s^{-1}$), is a measurable quantity ($\equiv -d[Ce^{IV}]_t/dt$), directly related to $i_{mix}$ via the expression,

$$r(t) = i_{mix}/F \quad (5)$$

The model parameter $E_{mix,t}$ can be obtained from a modified version of eqn. (3), i.e.

$$E_{mix,t} = E'_{Ce} + (RT/F)\ \ln\{k_1[Ce^{IV}]_t - r(t))/(r(t) + k_1[Ce^{III}]_t)\} \quad (6)$$

provided $k_1$, the first-order rate constant for reaction (1), when it is wholly diffusion-controlled, is known; all other parameters in eqn. (6) can be calculated from the particular absorbance–time profile associated with the kinetic run, given that in every kinetic run the initial concentrations of both $Ce^{IV}$ and $Ce^{III}$ are known. If the electrochemical model described above is applicable to reaction (1) it follows from eqn. (2) that for any specific kinetic run the subsequent plot of $E_{mix,t}$ versus $\log(r(t))$ will be a straight line of gradient $b$ and intercept $-b \times \log(r_w)$, where $r_w = [i_w \exp(-2.303 \times E'_w/b)]/F$, given $E'_w$ is the equilibrium redox potential of the $O_2/H_2O$ couple.

The electrochemical model of $O_2$ catalysis described above has been used to describe successfully the kinetics of reaction (1) mediated by $RuO_2 \cdot yH_2O$* [8]. From the results of this work a Tafel slope of 30 mV per decade was reported which was the same value found in electrochemical studies of water oxidation carried out using macro-anodes of films of highly defective ruthenium(IV) oxide [11, 13]. In contrast, similar electrochemical studies carried out on low defect $RuO_2$ film anodes, to which anhydrous $RuO_2$ is most akin, often reveal a Tafel slope of 40 mV per decade [11, 13]. Thus, assuming the same electrochemical model applies, the kinetics of reaction (1) mediated by anhydrous $RuO_2$ are likely to be noticeably different to those observed for $RuO_2 \cdot yH_2O$*.

## Results and discussion

*Determination of $k_1$ (in a medium of fixed [$HClO_4$] and [$H_2SO_4$]; low [$Ce^{IV}$])*

As noted above before the electrochemical model can be fully applied $k_1$, the first order rate constant when reaction (1) is wholly diffusion controlled, must first be determined. Equation (6) may be rewritten as follows:

$$i_{mix} = \frac{k_1 F\{[Ce^{IV}]_t - [Ce^{III}]_t \exp[F\Delta E/RT]\}}{1 + \exp[F\Delta E/RT]} \quad (7)$$

where $\Delta E = E_{mix,t} - E'_{Ce}$. From eqn. (7) it appears that the mixture current and, therefore, the rate, $r(t)$, will tend to that value expected for a diffusion controlled reaction, i.e.

$$i_{mix,t} = k_1 F[Ce^{IV}]_t \quad (8)$$

the more negative the value of $\Delta E$. According to the electrochemical model, diffusion controlled kinetics will also be favoured if the initial concentration of $[Ce^{IV}]$ is low and that of $[Ce^{III}]$ significantly lower again (preferably zero). The value of $\Delta E$ can be made more negative by increasing the value of $E'_{Ce}$ and this can be done by changing the acid medium from one in which the $Ce^{IV}$ and $Ce^{III}$ ions are highly complexed, such as $H_2SO_4$, to one in which they are not, such as $HClO_4$. Thus, in 0.5 mol $dm^{-3}$ $H_2SO_4$ the formal redox potential of the $Ce^{IV}/Ce^{III}$ couple is 1.44 V versus NHE whereas in 1 mol $dm^{-3}$ $HClO_4$ it is 1.70 versus NHE [14].

In the work associated with this section the stock dispersion (300 mg $dm^{-3}$) was made up in 1 mol $dm^{-3}$ $HClO_4$ and in a kinetic run, after mixing with the injected $Ce^{IV}$ solution at $t=0$, the overall acid medium was predominantly $HClO_4$ (0.965 mol $dm^{-3}$) with a relatively small but fixed concentration of $H_2SO_4$ (0.017 mol $dm^{-3}$) due to the 0.5 mol $dm^{-3}$ $H_2SO_4$ present in the injected $Ce^{IV}$ solution. The redox potential of the $Ce^{IV}/Ce^{III}$ couple in the 0.965 mol $dm^{-3}$ $HClO_4$ + 0.017 mol $dm^{-3}$ $H_2SO_4$ acid medium is 127 mV more positive than that in 0.5 mol $dm^{-3}$ $H_2SO_4$ and this, combined with the use of a low $[Ce^{IV}]$ and with $[Ce^{III}]_{t=0} = 0$ mol $dm^{-3}$, appears sufficient to cause $E_{mix,t}$ to lie in a region in which reaction (1) is diffusion controlled. Thus, with the injection of 90 $mm^3$ of a 0.01 mol $dm^{-3}$ $Ce^{IV}$ solution in 0.5 mol $dm^{-3}$ $H_2SO_4$ into the stock dispersion at 30 °C the resulting absorbance–time profile, illustrated in Fig. 1(a), when analysed for first-order kinetics (Fig. 1(b)) gives a good straight line over 2½ half-lives of gradient $-0.0400 \pm 0.0001$ $s^{-1}$ which is equal to $-k_1$ (at 30 °C).

In another set of experiments in the predominantly perchloric acid medium the concentration of $RuO_2$ was varied over the range 30 to 300 mg $dm^{-3}$ with all other conditions the same, i.e. $[Ce^{IV}]_{t=0} = 3.5 \times 10^{-4}$ mol $dm^{-3}$; $[Ce^{III}]_{t=0} = 0$ mol $dm^{-3}$; $T =$ 30 °C. From a first order analysis of each of the subsequent absorbance–time profiles generated a

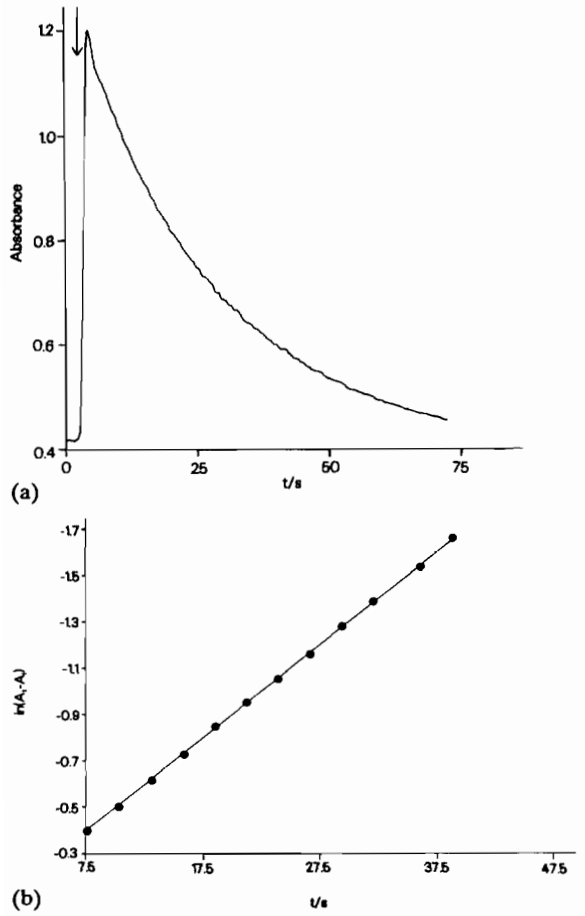


Fig. 1. Results of a kinetic study of reaction (1) mediated by anhydrous $RuO_2$ in which 90 $mm^3$ of a $Ce^{IV}$ solution (0.01 mol $dm^{-3}$ in 0.5 mol $dm^{-3}$ $H_2SO_4$) were injected into a dispersion of $RuO_2$ (2.5 $cm^3$; 300 mg $dm^{-3}$) in 1 mol $dm^{-3}$ $HClO_4$ at 30 °C. (a) Absorbance–time profile ($\lambda = 320$ nm), with arrow denoting point of injection. (b) First order analysis of the data contained in (a). A least-squares analysis of this data gives the following information: number of points ($n$) = 439, gradient ($m$) = $-0.0400 \pm 0.0001$ $s^{-1}$, intercept ($c$) = $-0.106 \pm 0.001$, correlation coefficient ($r$) = 0.9998.

series of $k_1$ values were obtained which when plotted in the form $k_1$ versus $[RuO_2]$ gives a good straight line as illustrated in Fig. 2. This finding appears to support the electrochemical model since the latter predicts that the mixture current, which is directly related to $k_1$, see eqn. (8), will depend directly upon the available surface area which, in our case, will depend upon $[RuO_2]$.

Further confirmation that reaction (1) is diffusion controlled in the largely $HClO_4$ medium was obtained from a study of the variation of $k_1$ as a function of temperature over the range 20–70 °C using the same reaction conditions as above, with $[RuO_2] = 300$ mg $dm^{-3}$. The Arrhenius plot of $\ln(k_1)$ versus $T^{-1}$ is illustrated in Fig. 3 and from a least-squares analysis

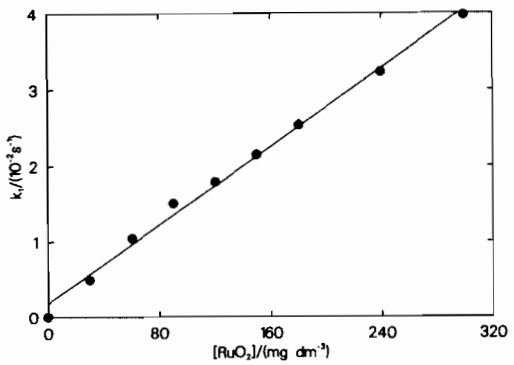


Fig. 2. Plot of $k$, vs. $[RuO_2]$ where the different values for $k_1$ were determined using a variety of different $[RuO_2]$ values but otherwise the same reaction conditions as in Fig. 1. A least-squares analysis of this data gives the following information: $n = 9$, $m = (1.29 \pm 0.04) \times 10^{-4}$ $dm^3$ $mg^{-1}$ $s^{-1}$, $c = (1.87 \pm 0.68) \times 10^{-3}$ $s^{-1}$, $r = 0.9962$.

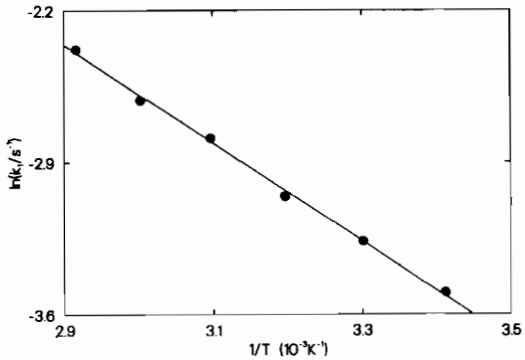


Fig. 3. Arrhenius plot where the different values for $k_1$ were determined in the predominantly $HClO_4$ medium for different temperatures but otherwise the same reaction conditions as in Fig. 1. A least-squares analysis of this data gives the following information: $n = 6$, $m = (-2.26 \pm 0.05) \times 10^3$ K, $c = 4.2 \pm 0.17$, $r = 0.9989$.

of the data an activation energy of $19 \pm 1$ kJ $mol^{-1}$ was calculated, which is in good agreement with that expected for a diffusion controlled reaction, i.e. 15–19 kJ $mol^{-1}$ [15, 16].

*Kinetics in a fixed [$H_2SO_4$] medium*

From the electrochemical model, partly diffusion controlled kinetics as described by eqn. (7), will be favoured if $\Delta E$ is small, $[Ce^{IV}]_{t=0}$ is high and $[Ce^{III}]_{t=0}$ is made higher still [17], and a good test of this prediction is the determination of the kinetics of reaction (1) under such conditions. Figure 4 illustrates the relative absorbance–time plots which resulted from a series of repeat injections of 90 $mm^3$ of a 0.1 mol $dm^{-3}$ $Ce^{IV}$ solution, in 0.5 mol $dm^{-3}$ $H_2SO_4$, into 2.5 $cm^3$ of a stock dispersion of $RuO_2$ (300 mg $dm^{-3}$ made up in 0.5 mol $dm^{-3}$ $H_2SO_4$) at 70 °C; the kinetics are very slow at 30 °C. The results illustrated in Fig. 4 are in qualitative agreement with

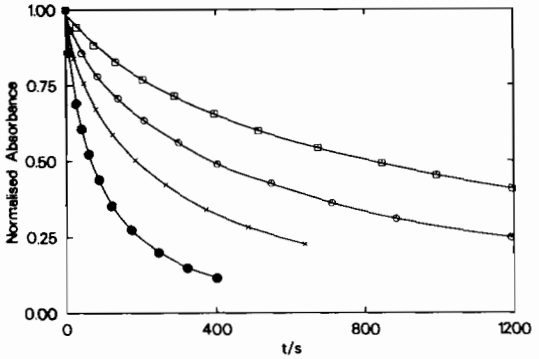


Fig. 4. Absorbance vs. time profiles ($\lambda = 430$ nm) arising from a kinetic study of reaction (1) mediated by anhydrous $RuO_2$ in which a series of repeat injections of 90 $mm^3$ of a $Ce^{IV}$ solution (0.01 mol $dm^{-3}$ in 0.5 mol $dm^{-3}$ $H_2SO_4$) were made into a dispersion of $RuO_2$ (2.5 $cm^3$; 300 mg $dm^{-3}$) in 0.5 mol $dm^{-3}$ $H_2SO_4$ at 70 °C. From left to right the decay curves are for the 1st to the 4th injection.

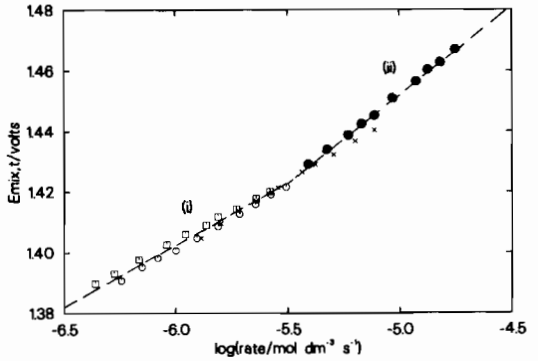


Fig. 5. Tafel plot of the data illustrated in Fig. 4. Values for $E_{mix,t}$ were calculated using eqn. (6) and a $k_1$ value of 0.0682 $s^{-1}$. A least-squares analysis of this data gives the following information: (i) $n = 30$, $m = 0.041 \pm 0.008$ V (decade)$^{-1}$, $c = 1.65 \pm 0.005$ V, $r = 0.9945$; (ii) $n = 10$, $m = 0.058 \pm 0.0006$ V (decade)$^{-1}$, $c = 1.75 \pm 0.003$ V, $r = 0.9995$.

eqn. (7) of the electrochemical model which predicts that the rate of reaction (1) should decrease with increasing $[Ce^{III}]$.

None of the absorbance–time profiles illustrated in Fig. 4 give a good fit to first order kinetics, but each can be successfully analysed using the electrochemical model. Thus, for each decay trace $r(t)$ and a corresponding value for $E_{mix,t}$ can be determined at any time $t$ during the reaction using eqn. (6). In the calculation of $E_{mix,t}$ a common value for $k_1$ is required and this was obtained from a first order analysis of the absorbance–time plot recorded at 70 °C and under the same acid conditions as used in the previous section since they favour wholly diffusion controlled kinetics for reaction (1); $k_1$ was taken as $= 0.0682$ $s^{-1}$. Analysis of the data contained in each decay trace illustrated in Fig. 4 using eqn. (6) of the electrochemical model gave rise to a series of different Tafel plots of $\log(r(t))$ versus $E_{mix,t}$ and these are collected together and illustrated in Fig. 5, from which it is apparent that the overall Tafel plot has two distinct slopes, namely 41 mV per decade at $E_{mix,t} < 1.42$ V versus NHE and 58 mV per decade at $E_{mix,t}$ values $> 1.42$ V versus NHE.

As noted previously, from electrochemical studies on the oxidation of water carried out by others using low defect $RuO_2$ film anodes, a Tafel slope of 40 mV per division was reported and subsequently interpreted in terms of the 'electrochemical oxide' pathway for water oxidation [11, 13], i.e.

$$S + H_2O \longrightarrow S\text{–}OH + H^+ + e^- \quad (9)$$

$$S\text{–}OH \longrightarrow S\text{–}O + H^+ + e^- \quad (10)$$

$$2S\text{–}O \longrightarrow 2S + O_2 \quad (11)$$

where S is the surface active site. It can be shown [10] that if either reaction (9), (10) or (11) is the rate determining step then, at low overpotentials, the resulting Tafel slope will be 120, 40 or 15 mV, respectively. Thus, from the results illustrated in Fig. 5 it would appear that at low potentials the oxidation of water mediated by anhydrous $RuO_2$ occurs via an 'electrochemical oxide' pathway with reaction (11) as the rate determining step. Interestingly, the 'electrochemical oxide' pathway predicts that at higher potentials the Tafel slope will tend to a value of 120 mV per decade as the number of surface active sites available tends to zero [11]. Thus, it is possible to explain the observed apparent Tafel slope of 58 mV per decade illustrated in Fig. 5 for potentials $> 1.41$ V versus NHE as simply indicative of the process of changing Tafel slope from 40–120 mV per decade as the total surface coverage by intermediates becomes significant.

The applicability of the electrochemical model and in particular eqn. (6) to our system was tested further through a series of experiments in which the reaction medium was once again 0.5 mol $dm^{-3}$ $H_2SO_4$ with the $[Ce^{IV}]_{t=0} = 3.5 \times 10^{-3}$ mol $dm^{-3}$, $[Ce^{IV}]_{t=0}/[Ce^{III}]_{t=0}$ ratio = 1:3 and the reaction temperature = 70 °C.

Using the reaction conditions described above, in one set of experiments the absorbance–time profiles arising from the decay of $Ce^{IV}$ ions via reaction (1) were recorded as a function of $[RuO_2]$ over the range 60–300 mg $dm^{-3}$ and the data subjected to analysis using eqn. (6) of the electrochemical model; the resulting Tafel type plots are illustrated in Fig. 6(a). For each run the value of $k_1$ used in eqn. (6) to determine the different values of $E_{mix,t}$ was taken as that determined using the same value of $[RuO_2]$

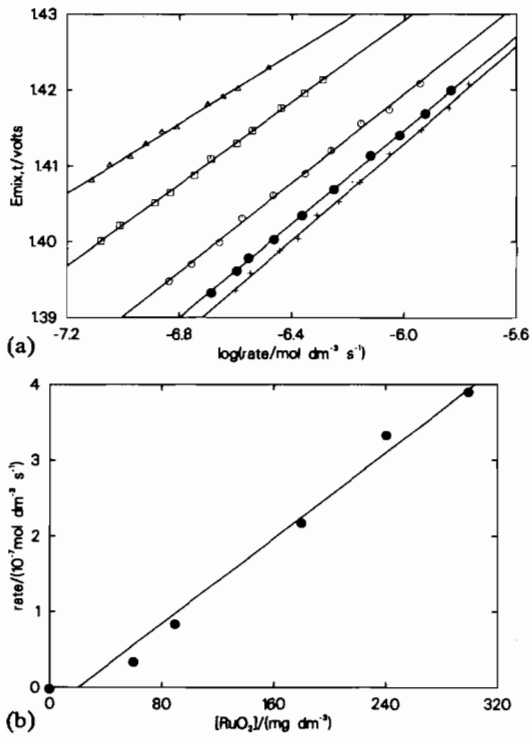


Fig. 6. (a) Tafel plots of the absorbance–time profiles generated in a study of the kinetics of reaction (1) mediated by anhydrous $RuO_2$ in which the concentration of $[RuO_2]$ was varied; all other reaction conditions as for Fig. 4, except $[Ce^{III}]_{t=0}$: $[Ce^{IV}]_{t=0}$ = 1:3. From left to right the Tafel plots correspond to $[RuO_2]$ values of 60, 90, 180, 240 and 300 mg $dm^{-3}$, respectively. (b) Plot of $r(t)$ vs. $[RuO_2]$, using $r(t)$ values read from (a) for $E_{mix,t}$ = 1.40 V vs. NHE. A least-squares analysis of this data gives the following information: $n = 6$, $m = (1.41 \pm 0.09) \times 10^{-9}$ mol $mg^{-1}$ $s^{-1}$, $c = (-2.84 \pm 1.68) \times 10^{-8}$ mol $dm^{-3}$ $s^{-1}$, $r = 0.9912$.

in a parallel set of identical experiments carried out in the largely $HClO_4$ medium described in the previous section. From the electrochemical model it is predicted that the collection of Tafel slopes illustrated in Fig. 6(a) can be used to determine the value of $r(t)$ at any arbitrarily chosen fixed potential for each kinetic run and that a subsequent plot of $r(t)$ versus $[RuO_2]$ will be a straight line, since under these conditions $r(t)$ will reflect simply the direct dependence of $i_{mix,t}$ upon catalyst surface area and, therefore, $[RuO_2]$. Using the data illustrated in Fig. 6(a) the plot of $r(t)$ versus $[RuO_2]$ for $E_{mix,t}$ = 1.40 V versus NHE does indeed give a good straight line as illustrated in Fig. 6(b).

In a second series of experiments the kinetics of reaction (1) were studied as a function of temperature over the range 30–70 °C using the same reaction conditions as before, with $[RuO_2]$ = 300 mg $dm^{-3}$. For each kinetic run the value of $k_1$ used to determine the different values of $E_{mix,t}$ using eqn. (6) was taken as that determined for the same temperature in an identical experiment, but carried out in the largely $HClO_4$ medium. The resulting Tafel plots of the data and subsequent Arrhenius plot of $\ln(r(t))$ versus $T^{-1}$ ($E_{mix,t}$ = 1.4 versus NHE) are illustrated in Fig. 7(a) and (b), respectively. From the gradient of the Arrhenius plot illustrated in Fig. 7(b) a value for the activation energy (for the oxidation of water to $O_2$ on particles of anhydrous $RuO_2$) of 46 ± 5 kJ $mol^{-1}$ was calculated, which compares well with the value of 50.4 kJ $mol^{-1}$ reported in a previous electrochemical study in which $RuO_2$ was used as the anode [18].

*Kinetics in an acid medium with different $[H_2SO_4]$/ $[HClO_4]$ ratios*

As noted earlier it is not only the presence of $Ce^{IV}$ ions which appears to inhibit the rate of reaction (1), but also that of sulfate ions which complex with the $Ce^{IV}$ ions thereby reducing the formal redox

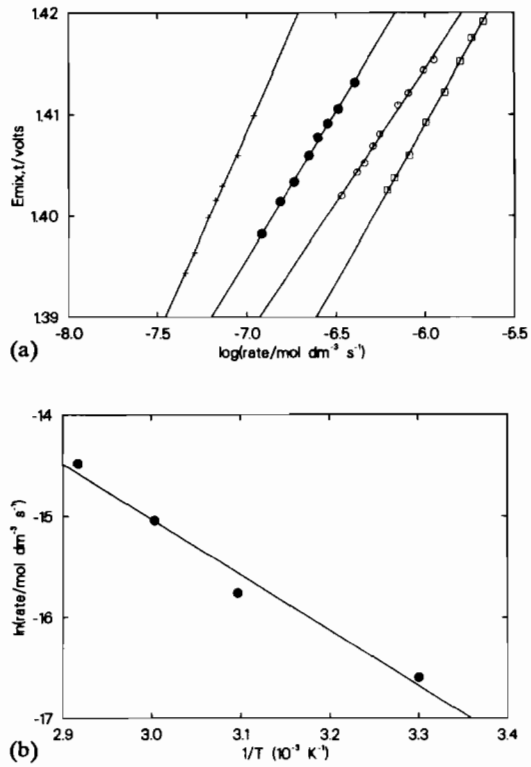


Fig. 7. (a) Tafel plots of the absorbance–time profiles generated in a study of the kinetics of reaction (1) mediated by anhydrous $RuO_2$ in which the reaction temperature was varied; all other reaction conditions as for Fig. 6. From left to right the Tafel plots correspond to temperature values of 30, 50, 60 and 70 °C, respectively. (b) Plot of $\ln(r(t))$ vs. $T^{-1}$, using $r(t)$ values read from (a) for $E_{mix,t}$ = 1.40 V vs. NHE. A least-squares analysis of this data gives the following information: $n = 4$, $m = (-5.48 \pm 0.60) \times 10^3$ K, $c = 1.40 \pm 0.18$, $r = 0.9883$.

potential of the $Ce^{IV}/Ce^{III}$ couple [14]. As an illustration of this latter effect a series of absorbance–time profiles, illustrated in Fig. 8(a), were recorded for a variety of different $[H_2SO_4]/[HClO_4]$ ratios ranging from 0.063:1 to 0.5:0 using a fixed initial $[Ce^{IV}]/[Ce^{III}]$ ratio of 1:3 with $[Ce^{IV}]_{t=0} = 3.5 \times 10^{-3}$ mol $dm^{-3}$, $[RuO_2] = 300$ mg $dm^{-3}$ and $T = 70$ °C. In all cases the parameter $(2[H_2SO_4] + [HClO_4]) = 1$ mol $dm^{-3}$. In each different acid medium used the formal redox potential of the $Ce^{IV}/Ce^{III}$ couple was determined and each was used in the calculation of the $E_{mix,t}$ values for the appropriate kinetic run. The resulting Tafel plots are illustrated in Fig. 8(b) and the overall image is similar to that illustrated in Fig. 6(b) with two slopes 40 and 52 mV per decade, respectively. These findings are as expected from the electrochemical model given its applicability to this system.

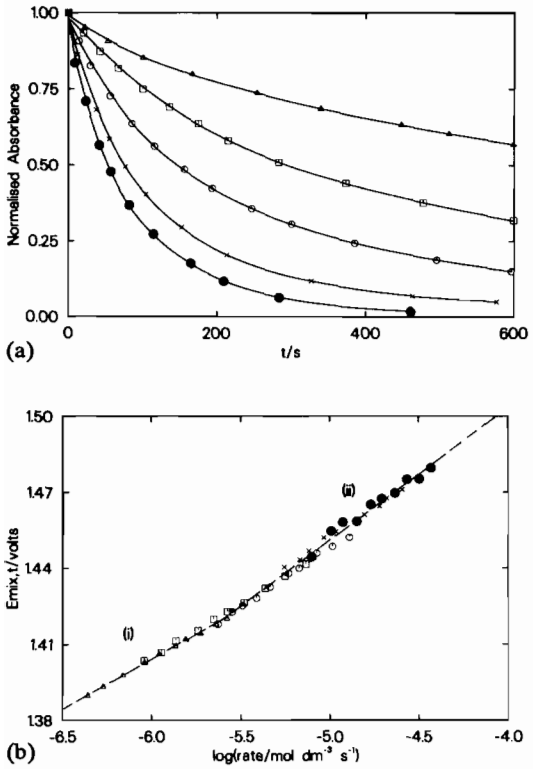


Fig. 8. (a) Absorbance vs. time profiles ($\lambda = 430$ nm) in which 90 $mm^3$ of the same $Ce^{IV}$ solution (0.1 mol $dm^{-3}$ in 0.5 mol $dm^{-3}$ $H_2SO_4$) was injected into a catalyst dispersion of $RuO_2$ (2.5 $cm^3$; 300 mg $dm^{-3}$) made up in an acid solution containing different $[H_2SO_4]/[HClO_4]$ ratios (with $2 \times [H_2SO_4] + [HClO_4] = 1$ mol $dm^{-3}$). The curves correspond, from left to right, to $[H_2SO_4]$ of: 0.063, 0.1, 0.2, 0.3 and 0.5 mol $dm^{-3}$, respectively. (b) Tafel plot of the data illustrated in (a). Values for $E_{mix,t}$ were calculated using eqn. (6) and a $k_1$ value of 0.0682 $s^{-1}$. A least-squares analysis of this data gives the following information: (i) $n = 16$, $m = 0.040 \pm 0.001$ V (decade)$^{-1}$, $c = 1.64 \pm 0.006$ V, $r = 0.9957$; (ii) $n = 34$, $m = 0.052 \pm 0.001$ V (decade)$^{-1}$, $c = 1.71 \pm 0.005$ V, $r = 0.9932$.

## Conclusions

Reaction (1) is catalysed by anhydrous $RuO_2$ in a variety of different acid media. The observed kinetics of catalysis are readily interpreted using an electrochemical model in which a Nernstian reduction reaction ($Ce^{IV} \rightarrow Ce^{III}$) is coupled to a highly irreversible oxidation reaction ($H_2O \rightarrow 2H^+ + \frac{1}{2}O_2$) via microelectrode particles of anhydrous $RuO_2$. The observed kinetics of reaction (1) in 0.5 mol $dm^{-3}$ $H_2SO_4$, when analysed using this electrochemical model, indicate that the oxidation of water occurs via an 'electrochemical oxide' pathway with an overall activation energy of $46 \pm 5$ kJ $mol^{-1}$. This electrochemical model may find further application in interpreting the kinetics arising from studies of other redox catalyst systems and, possibly, systems in which the 'catalyst' undergoes corrosion.

## Acknowledgement

We thank the SERC for supporting this work.

## References

1 M. Grätzel (ed.), *Energy Resources through Photochemistry and Catalysis*, Academic Press, New York, 1983.
2 A. Mills, *Sci. Tech. Rev. (Univ. Wales), 4* (1988) 39.
3 A. Mills, *Chem. Soc. Rev., 18* (1989) 285.
4 A. Mills, S. L. Giddings and I. Patel, *J. Chem. Soc., Faraday Trans. 1, 83* (1987) 2317.
5 A. Mills, S. L. Giddings, I. Patel and C. Lawrence, *J. Chem. Soc., Faraday Trans. 1, 83* (1987) 2331.
6 A. Mills, *J. Chem. Soc., Dalton Trans.*, (1982) 1213.
7 A. Mills and T. Russell, *J. Chem. Soc., Faraday Trans. 1, 87* (1991) 1245.
8 A. Mills and N. McMurray, *J. Chem. Soc., Faraday Trans. 1, 85* (1989) 2055.
9 M. Spiro, *Chem. Soc. Rev., 15* (1986) 141.
10 J. O'M. Bockris, *J. Phys. Chem., 24* (1956) 817.
11 S. Trasatti and G. Lodi, in S. Trasatti (ed.), *Electrodes of Conductive Metallic Oxides*, Part B, Elsevier, Amsterdam, 1980, and refs. therein.
12 A. J. Bard and L. R. Faulkner, *Electrochemical Methods*, Wiley, London, 1980, p. 29.
13 S. Trasatti and W. E. O'Grady, *Adv. Electrochem. Electrochem. Eng., 12* (1981) 177.
14 E. Wadsworth, F. R. Duke and C. A. Goetz, *Anal. Chem., 29* (1957) 1824.
15 F. Wilkinson, *Chemical Kinetics and Reaction Mechanisms*, Van Nostrand Reinhold, London, 1981, p. 140.
16 J. W. Moore and R. G. Pearson, *Kinetics and Mechanism*, Wiley, New York, 1981, p. 239.
17 A. Mills and N. McMurray, *J. Chem. Soc., Faraday Trans. 1, 85* (1989) 2047.
18 G. Lodi, A. Sivieri, A. DeBattisti and S. Trasatti, *J. Appl. Electrochem., 8* (1978) 135.